Nondestructive, Indirect Assessment of the Biomechanical Properties of the Rat Intervertebral Disc Using Contrast-Enhanced μCT

Michael D. Newton,[1] Samantha E. Hartner,[1] Karissa Gawronski,[1] Erik J. Davenport,[2] Shannon C. Timmons,[2] Kevin C. Baker,[1,3] Tristan Maerz[1,3,4]

[1]Orthopaedic Research Laboratory, Beaumont Health, Royal Oak, Michigan, [2]Department of Natural Sciences, Lawrence Technological University, Southfield, Michigan, [3]Department of Orthopaedic Surgery, Oakland University – William Beaumont School of Medicine, Rochester, Michigan, [4]Department of Orthopaedic Surgery, University of Michigan, 109 Zina Pitcher Place, 48109 Ann Arbor, Michigan

Received 20 July 2017; accepted 24 December 2017
Published online 4 January 2018 in Wiley Online Library (wileyonlinelibrary.com). DOI 10.1002/jor.23850

ABSTRACT: Mechanical characterization of the intervertebral disc involves labor-intensive and destructive experimental methodology. Contrast-enhanced micro-computed tomography is a nondestructive imaging modality for high-resolution visualization and glycosaminoglycan quantification of cartilaginous tissues. The purpose of this study was to determine whether anionic and cationic contrast-enhanced micro-computed tomography of the intervertebral disc can be used to indirectly assess disc mechanical properties in an ex vivo model of disc degeneration. L3/L4 motion segments were dissected from female Lewis rats. To deplete glycosaminoglycan, samples were treated with 0 U/ml (Control) or 5 U/ml papain. Contrast-enhanced micro-computed tomography was performed following incubation in 40% Hexabrix (anionic) or 30 mg I/ml CA^{4+} (cationic) for 24 h ($n = 10$/contrast agent/digestion group). Motion segments underwent cyclic mechanical testing to determine compressive and tensile modulus, stiffness, and hysteresis. Glycosaminoglycan content was determined using the dimethylmethylene blue assay. Correlations between glycosaminoglycan content, contrast-enhanced micro-computed tomography attenuation, and mechanical properties were assessed via the Pearson correlation. The predictive accuracy of attenuation on compressive properties was assessed via repeated random sub-sampling cross validation. Papain digestion produced significant decreases in glycosaminoglycan content and corresponding differences in attenuation and mechanical properties. Attenuation correlated significantly to glycosaminoglycan content and to all compressive mechanical properties using both Hexabrix and CA^{4+}. Predictive linear regression models demonstrated a predictive accuracy of attenuation on compressive modulus and stiffness of 79.8–86.0%. Contrast-enhanced micro-computed tomography was highly predictive of compressive mechanical properties in an ex vivo simulation of disc degeneration and may represent an effective modality for indirectly assessing disc compressive properties.
© 2018 Orthopaedic Research Society. Published by Wiley Periodicals, Inc. J Orthop Res 36:2030–2038, 2018.

Keywords: intervertebral disc; contrast-enhanced micro-computed tomography; disc biomechanics; degenerative disc disease

Intervertebral disc (IVD) degeneration, and its resulting disability, represent an enormous global health burden. Low back pain, which can result from degenerative disc disease (DDD), is responsible for over $200 billion in health expenditures and lost wages in the United States alone.[1] IVD degeneration and its root cause have been difficult to define. Genetic predisposition, aging, impedance of nutrient transport, changes to extracellular matrix (ECM) structure and composition, acute injury, and heavy loading have all been identified as potential factors in the onset and progression of DDD.[2] Here, we focus on one of the early biochemical indicators of DDD,—the loss of sulfated glycosaminoglycan (GAG) from the intervertebral disc (IVD). It is unknown whether GAG loss is a causative factor in DDD, or a symptom of degeneration initiated by some other physiological process. Regardless, depletion of negatively-charged GAG contributes to an irreversible degenerative cascade by reducing hydrostatic pressure in the nucleus pulposus (NP) and compromising axial load distribution throughout the IVD, leading to focal overloading, damage, and ultimately, the progressive degeneration of IVD tissues.[3,4]

The biomechanical properties of the IVD are largely dependent on the structure and function of the GAG-rich extracellular matrix (ECM). During normal activity, the spine is subjected to highly variable axial loads—human L3/L4 discs have been reported to experience loads equivalent to 250% of total body weight—and the IVD is uniquely adapted to withstand this loading.[5] A healthy IVD is adequately hydrated, containing up to 80% water in the NP,[6] where the majority of GAG is concentrated. When axially compressed, the hydrostatic internal pressure in the NP redistributes the load radially to the collagen-rich lamellar fibers of the annulus fibrosus (AF), which resist radial tension, resulting in effective load transmission across the IVD.[7] The inner AF contains a considerable concentration of GAG and is also capable of some direct resistance to axial compression via its own internal pressure.[4,8] Studies of cadaveric IVDs have demonstrated significant correlations of GAG content to NP swelling stress and aggregate modulus, and decreases in GAG content are associated with increasing age and increasing IVD degeneration score.[9] In preclinical models of IVD degeneration, IVD injury has been shown to reduce compressive properties,[10] and GAG concentration in the NP has been shown to significantly correlate to compressive stiffness and range of motion in cyclic tension/compression tests.[4]

Grant sponsor: Department of Orthopaedic Surgery at Beaumont Health; Grant sponsor: Department of Natural Sciences at Lawrence Technological University.
Correspondence to: Tristan Maerz, (T: +734-936-2566, F: +734-232-9622; E-mail: tmaerz@umich.edu)
© 2018 Orthopaedic Research Society. Published by Wiley Periodicals, Inc.

Small animal models of DDD have played an increasingly important role in understanding pathology, as well as testing new regenerative medicine-based strategies.[6,11,12] The experimental determination of IVD mechanical properties in these small animal models is both labor-intensive and destructive. The process usually involves careful dissection to isolate the motion segment, irreversible embedding of the vertebral bodies, meticulous mounting on a materials testing system, and a potentially-lengthy testing protocol. Given the destructive and time-intensive nature of IVD mechanical testing, a minimally-invasive, rapid assessment of IVD mechanical properties is of significant interest for both preclinical and clinical applications.

Contrast-enhanced micro-computed tomography (CE-μCT) is a nondestructive tool for high-resolution visualization and GAG quantification of cartilaginous tissues.[13–17] Our group has recently demonstrated the use of both anionic and cationic contrast agent-enhanced μCT for the 3D visualization and molecular characterization of the IVD,[18] and we have previously shown that anionic CE-μCT is a sensitive tool for the ex vivo assessment of DDD in a rabbit model.[14] Lakin et al[19–21] have demonstrated a local correlation of CE-μCT attenuation to compressive modulus and coefficient of friction in articular cartilage, exhibiting the utility of CE-μCT for the mechanical characterization of cartilaginous tissues. GAG content plays a similarly important role in the compressive mechanics of articular cartilage and IVD tissue. However, compressive load distribution across the entire vertebra-disc-vertebra motion segment is much more mechanically complex compared to the local compression of articular cartilage tissue, and thus it is unknown whether a similar correlation between CE-μCT attenuation and compressive properties exists in the IVD. As such, the purpose of this study was to assess the use of CE-μCT to nondestructively characterize the mechanical properties of the IVD by establishing correlations of anionic and cationic CE-μCT attenuation to experimentally determined biomechanical properties in healthy and degenerate rat lumbar IVDs.

METHODS

Specimen Preparation and Enzyme-Mediated Digestion

IACUC approval was not required for this study, as all described methodology was performed post mortem. All specimens were obtained from animals used in an unrelated, IACUC-approved protocol. Skeletally mature, female Lewis rats aged 14–20 weeks (~200–220 g) were euthanized via CO_2 asphyxiation. Lumbar spines were dissected en bloc and fresh frozen until dissection according to a previously described protocol.[18] To ensure that the spines would fit uniformly into a custom cutting jig, the transverse processes and pedicle fragments were removed using a die grinder equipped with a sanding drum attachment, which was able to remove bone without inducing concomitant fractures. Each specimen was then secured in the cutting jig and transverse cuts were made through the L3 and L4 vertebral bodies to isolate the L3/L4 motion segment. The cutting jig facilitated two parallel cuts through the vertebral bodies to ensure that applied loads were uniformly axial and consistent between specimens. Specimens were then randomized to one of two contrast agent groups (Hexabrix and CA^{4+}) and further randomized to one of two enzymatic digestion groups (0 or 5 U/ml) ($n = 10$ per group per enzyme concentration). Hexabrix (ioxaglate) was acquired commercially (Hexabrix 320, Guerbet, Inc., Bloomingdale, IN), while CA^{4+} was synthetically prepared using a protocol adapted from Joshi et al[22] (Supplemental Information). To deplete GAG content, enzymatic digestion was induced by incubation in phosphate-buffered saline (PBS, pH = 7.4) containing 0 or 5 U/ml papain (Sigma–Aldrich, St. Louis, MO) for 24 h at 37°C, as previously described.[18,23,24] In an earlier study, 5 U/ml papain was determined to induce significant reduction in GAG concentration while leaving the NP and AF structures intact and distinguishable via μCT and gross observation under a microscope.[18]

Contrast Agent Incubation and μCT Imaging

Contrast agent solutions containing 40% Hexabrix (Guerbet, LLC) and 30 mg I/ml CA^{4+} were prepared according to a previously described protocol.[18] These contrast agent concentrations were previously determined to provide optimal contrast enhancement for morphological and compositional analysis of rat IVDs. Immediately following enzyme-mediated digestion, specimens were incubated in contrast agent for 24 h at room temperature. The motion segments were secured in a custom sample holder containing humidifying silica beads to maintain a 70% humid environment, and the IVDs were imaged on a μCT imaging system (μCT-40, Scanco Medical AG, Brüttisellen, Switzerland) at 55 kVp, 145 μA, 250 ms integration time, with an isotropic voxel size of 20 μm. The cross-sectional area (CSA) of each IVD was calculated from a three-dimensional (3D) volume of interest (VOI) manually contoured by an experienced investigator (SEH, KG) using a custom MATLAB 3-plane viewing interface. Attenuation data was calculated from the IVD VOI along with an additional NP VOI that was manually contoured. Contours were checked for accuracy by two additional investigators (MDN, TM). Individual disc heights were calculated using a custom MATLAB program to manually delineate the endplate borders and calculate the average distance between consistent anatomical locations.

Mechanical Testing and Data Analysis

Non-destructive, uniaxial, cyclic compression-tension testing was performed to determine the mechanical properties of the IVDs. Using cyanoacrylate, motion segments were secured between rigid, parallel aluminum platens on a materials testing system equipped with a 250 N load cell (Insight 5, MTS, Eden Prairie, MN). Each end of the motion segment was secured within a shallow trough within each platen, enabling the cyanoacrylate to pool around the ends of the specimen and create a pot to ensure secure fixation. Preliminary testing confirmed that this fixation scheme was able to support both compressive and tensile loads at up to double those experienced during testing. During mechanical testing, the IVDs were immersed in room temperature saline supplemented with 1X protease inhibitors and 1% penicillin/streptomycin with fungizone (Thermo Fisher Scientific, Waltham, MA). Mechanical loading was performed as previously described.[4,12,25] A 1 N preload was applied for 30 min, followed by 20 sinusoidal loading cycles from 4.5 N

compression to 3 N tension at 0.1 Hz. Data from the 20th cycle was analyzed. Load and extension values were converted to stress and strain using individually determined IVD CSA and height. Compressive and tensile moduli were defined as the slope of the linear compressive and tensile regions of the stress/strain curve, respectively, which were isolated using MATLAB. An algorithm was employed which facilitated manual selection of the compressive and tensile regions of the 20th testing cycle, as well as the linear region of each stress/strain curve. The neutral point delineating the compressive and tensile regions of the cycle was defined as the midpoint between the two points on the cycle at which zero stress was recorded.[26] Compressive, tensile, and total hysteresis was calculated as the area under the stress/strain curve for the respective portion of the cycle.

Biochemical Quantification of GAG Content

Prior to GAG quantification, each IVD was rinsed for 20 h in room-temperature PBS to remove residual contrast agent. IVDs were then meticulously dissected from the vertebral endplates using microscopy-guided dissection and lyophilized for 2 h. The desiccated IVDs were kept in storage at −80°C prior to batch processing using a 1,9-dimethylmethylene blue (DMMB) assay. IVDs were digested in a 50 μg/ml proteinase K solution for 20 h and the DMMB assay was performed as previously described.[18] A standard curve was generated using solutions containing 0–70 μg/ml chondroitin sulfate (CS).

Statistical Analysis

All statistical analysis was performed using SPSS (v22.0, IBM, Armonk, NY). Correlations between variables were assessed using the Pearson product moment correlation. To assess differences between testing groups, a two-way analysis of variance (ANOVA) was applied as follows: Normality and equality of variances were assessed using Shapiro–Wilk and Levene's tests, respectively. There were no significant violations of normality. However, several variables exhibited highly unequal variances. Variables which met the assumption of equal variances were assessed using a standard two-way ANOVA. Variables which significantly violated the assumption of equal variances underwent log transformation, were reassessed to confirm that the transformed data exhibited equality of variances, and then the transformed data was analyzed via two-way ANOVA. Log transformation was performed on the following variables: IVD, NP, and AF attenuation, tensile stiffness, tensile modulus, total strain, and compressive, tensile, and total hysteresis. Regardless of whether log transformation was employed for statistical analysis, all aggregate data was reported in terms of the untransformed mean and 95% confidence interval.

The predictive accuracy of contrast-enhanced attenuation on compressive mechanical properties was assessed across 100 iterations of repeated random sub-sampling cross validation. At each iteration, datasets from each contrast agent were randomly split into evenly sized training and validation sets ($n = 10$ training samples; $n = 10$ validation samples). Within each set, there was an even distribution of undigested and digested samples to avoid model bias. The mean absolute percentage error (MAPE) between predicted and actual values was calculated as follows:

$$\mathrm{MAPE} = \frac{100}{n}\sum \frac{|y_{\mathrm{pred}} - y_{\mathrm{exp}}|}{y_{\mathrm{exp}}}$$

MAPE was averaged across the 100 iterations of cross validation and reported for each model combination.

RESULTS

There were no significant differences in CSA (Hexabrix: 7.51 [7.36, 7.65] mm^2; CA^{4+}: 7.60 [7.35, 7.84] mm^2, $p = 0.526$) or post-preload IVD height (Hexabrix: 1.04 [0.98, 1.09] mm; CA^{4+}: 1.04 [0.99, 1.08] mm, $p = 0.945$) between samples in the Hexabrix and CA^{4+} groups. Furthermore, there were no significant differences in CSA between undigested (0 U/ml papain) and digested samples (5 U/ml papain) in the Hexabrix group (0 U/ml: 7.60 [7.38, 7.81] mm^2; 5 U/ml: 7.41 [7.19, 7.65], $p = 0.362$) or CA^{4+} group (0 U/ml: 7.70 [7.35, 8.05] mm^2; 5 U/ml: 7.49 [7.09, 7.88] mm^2, $p = 0.263$). Within the Hexabrix group, post-preload IVD height was significantly lower in digested IVDs (0 U/ml: 1.10 [1.06, 1.13] mm; 5 U/ml: 0.98 [0.95, 1.01] mm, $p < 0.001$), but no significant differences were observed within the CA^{4+} group, although digested IVDs exhibited slightly lower mean height (0 U/ml: 1.05 [1.01, 1.09] mm; 5 U/ml: 1.02 [0.96, 1.08] mm, $p = 0.224$). Enzymatic digestion induced significant decreases in total GAG content in both contrast agent groups (Table 1). As expected, corresponding changes in the attenuation profile of the whole IVD and the NP were measured due to digestion in both contrast agent groups, with IVDs in the Hexabrix group exhibiting significant increases in attenuation and IVDs in the CA^{4+} group exhibiting significant decreases in attenuation (Table 1). In the Hexabrix group, digested IVDs exhibited 36.6% higher whole IVD attenuation and 33.6% higher NP attenuation compared to undigested IVDs (Fig. 1A and B). In the CA^{4+} group, digested IVDs exhibited 28.5% lower whole IVD attenuation and 31.5% lower NP attenuation compared to undigested IVDs (Fig. 1C and D). Enzymatic digestion induced significant changes in the mechanical properties of IVDs in both contrast agent groups; digested IVDs had significantly lower compressive modulus and stiffness, tensile modulus and stiffness, and significantly higher compressive and total hysteresis compared to undigested IVDs (Table 2). Digested IVDs in the Hexabrix group also exhibited significantly higher tensile hysteresis, though this difference was not observed in the CA^{4+} group (Table 2).

Strong linear correlations were observed between GAG content, μCT attenuation, and mechanical properties in both contrast agent groups. Total GAG content correlated significantly to whole IVD attenuation and NP attenuation in both Hexabrix and CA^{4+} groups (Fig. 2), and significantly to compressive modulus in both groups separately (Hexabrix: $r = 0.914$, $p < 0.001$; CA^{4+}: $r = 0.811$, $p < 0.001$) and when aggregating all IVDs together (Fig. 3A). Weaker, albeit significant, correlations were observed between GAG content and tensile modulus (Hexabrix: $r = 0.853$, $p < 0.001$; CA^{4+}: $r = 0.565$, $p = 0.009$).

Both whole IVD and NP attenuation correlated strongly to several mechanical properties (Table 3).

Table 1. CE-μCT Attenuation and GAG Content of IVDs

Contrast Agent	Papain (U/ml)	Mean CE-μCT Attenuation (HU)			GAG Content (μg CS)
		Whole IVD	NP	AF	
Hexabrix	0	3559 [3430, 3688]	2807 [2691, 2923]	3784 [3643, 3926]	49.9 [44.6, 55.2]
	5	4860 [4698, 5021]	3750 [3606, 3894]	5195 [5018, 5371]	18.1 [16.9, 19.3]
CA^{4+}	0	2636 [2537, 2735]	3571 [3422, 3721]	2290 [2167, 2412]	43.9 [39.2, 48.6]
	5	1884 [1831, 1937]	2447 [2376, 2518]	1688 [1629, 1747]	21.6 [19.9, 23.2]
Hexabrix	0 v. 5	$p < 0.001$	$p < 0.001$	$p < 0.001$	$p < 0.001$
CA^{4+}	0 v. 5	$p < 0.001$	$p < 0.001$	$p < 0.001$	$p < 0.001$

Data expressed as mean [95% confidence interval].

As the same trends were observed in both whole IVD and NP attenuation, and NP attenuation was more strongly correlated to most mechanical parameters, only correlations to NP attenuation will be discussed here. In the Hexabrix group, NP attenuation correlated strongly to compressive (Fig. 4A) and tensile modulus, compressive, and tensile stiffness (Table 3), and compressive, tensile, and total hysteresis (Fig. 4B, Table 3). In the CA^{4+} group, NP attenuation correlated strongly to compressive modulus (Fig. 4A), compressive stiffness (Table 3), compressive and total hysteresis (Fig. 4B, Table 3), but interestingly there was only a weak (though significant) correlation to tensile modulus, a weak, non-significant correlation to tensile stiffness, and no appreciable correlation to tensile hysteresis (Table 3).

MAPE values of predictive linear regression models using Hexabrix ranged from 14.05% to 17.63% (Table 4), and MAPE values of linear regression models using CA^{4+} ranged from 16.79% to 20.23% (Table 4), demonstrating an overall predictive accuracy of the use of CE-μCT to determine the compressive stiffness or modulus of the IVD to be ~80–86%. Using NP attenuation to predict compressive properties generally yielded lower MAPE values compared to using whole-IVD attenuation.

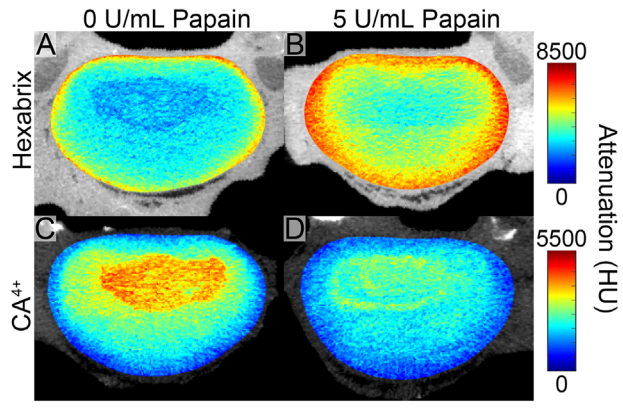

Figure 1. Representative colormaps of contrast-enhanced IVD attenuation imaged with either Hexabrix (A, B) or CA^{4+} (C, D) following a 24 h incubation in either saline (A, C) or 5 U/ml papain (B, D).

DISCUSSION

The biomechanical assessment of the IVD is important for disease characterization and the development of potential treatment strategies, but it is ultimately limited by its complex, time-consuming, and often destructive nature. In this study, the ability to employ CE-μCT for the nondestructive assessment of rodent IVD mechanical properties was demonstrated. Strong, highly significant linear correlations between CE-μCT attenuation and IVD mechanical properties were observed in an ex vivo model of IVD degeneration. CE-μCT attenuation correlated strongly to compressive mechanical properties and moderately, though significantly, to tensile properties. Linear regressions were established, which predicted disc mechanical properties based on IVD and NP attenuation, and the accuracy of these regressions as predictors of compressive stiffness and modulus was calculated using cross validation and found to be 79.8–86%.

The transmission and absorption of intervertebral/transvertebral compressive loading is a primary function of the IVD, and correspondingly CE-μCT attenuation correlated most strongly to compressive properties of the disc. Compressive modulus and stiffness of the IVD are primarily derived from hydrostatic pressure produced by GAG-mediated water retention, and its interaction with the highly organized lamellar structure of the AF.[5,7] Hysteretic behavior in cartilaginous tissues such as the IVD arises from their inherent viscoelasticity, which has been suggested to arise in part from water extravasation and imbibition during loading.[27,28] Thus, compressive modulus, stiffness, and hysteresis are all directly related to GAG and water content within the IVD. Both modalities of CE-μCT utilized in this study are highly sensitive to IVD GAG content,[14,18] and we demonstrated that CE-μCT attenuation correlated strongly to both compressive modulus and compressive stiffness of the IVD. Using cross validation modeling, we found that CE-μCT attenuation of the IVD was 80–86% accurate in predicting compressive stiffness and modulus, indicating a potential future role for CE-μCT as a surrogate for direct mechanical measurement in pathophys iological and regenerative studies. As our investigation employed an ex vivo model of enzymatic digestion to

Table 2. Mechanical Properties of IVDs

		Modulus (MPa)		Stiffness (N/mm)		Hysteresis ($\times 10^{-3}$ MPa)		
Contrast Agent	Papain (U/ml)	Compressive	Tensile	Compressive	Tensile	Compressive	Tensile	Total
Hexabrix	0	23.8 [22.4, 25.3]	7.0 [6.3, 7.6]	169 [160, 178]	51 [47, 54]	3.3 [2.7, 3.9]	4.3 [4.7, 3.9]	7.6 [6.6, 8.5]
	5	13.1 [10.9, 15.4]	5.0 [4.5, 5.4]	104 [88, 120]	42 [38, 45]	14.0 [11.3, 16.6]	10.5 [12.4, 8.5]	24.4 [20.1, 28.7]
CA^{4+}	0	21.9 [20.5, 23.4]	5.6 [4.7, 6.5]	168 [154, 181]	48 [40, 55]	7.7 [6.3, 9.1]	9.9 [11.3, 8.4]	17.6 [15.2, 20.0]
	5	11.4 [8.8, 14.1]	4.7 [4.3, 5.1]	88 [70, 105]	40 [36, 44]	18.0 [15.2, 20.8]	10.6 [12.1, 9.1]	28.6 [24.8, 32.5]
Hexabrix	0 v. 5	**$p < 0.001$**	***$p < 0.001$***	**$p < 0.001$**	**$p = 0.010$**	**$p < 0.001$**	**$p < 0.001$**	**$p < 0.001$**
CA^{4+}	0 v. 5	**$p < 0.001$**	**$p = 0.029$**	**$p < 0.001$**	**$p = 0.029$**	**$p < 0.001$**	$p = 0.411$	**$p < 0.001$**

Data expressed as Mean [95% confidence interval].

mimic the degenerative state of the IVD, future studies need to confirm this level of predictive accuracy in in vivo models of IVD degeneration.

CE-μCT attenuation also correlated significantly to IVD tensile properties—primarily tensile modulus—though predictably, these correlations were not as strong as those observed with compressive mechanical properties. The relationship between IVD tensile behavior and GAG content is not as well-established as in the case of compressive behavior. Furthermore, while the tensile properties of individual AF fibers and the tensile properties responsible for resisting radial expansion are well understood, uniaxial tensile properties of the whole IVD are not well characterized. Tensile properties of the IVD derive from the highly organized fiber structure of the AF, along with the Sharpey's fibers which anchor the IVD to the endplates, and also likely arise in part from IVD interstitial pressure and are therefore affected by GAG depletion, dehydration, and depressurization.[29–32] In addition to their role in water retention, GAG molecules can serve as matrix linkers,[7] and thus GAG digestion may directly destabilize the AF matrix. Finally, the broad-spectrum activity of papain utilized in our study likely also results in partial digestion of other AF matrix molecules, diminishing both compressive and tensile properties, though previous work suggests that the concentration of papain used in this study largely preserves AF structure.[23] Interestingly, CA^{4+} attenuation correlated markedly poorer to tensile properties compared to Hexabrix attenuation, though no difference was noted in compressive correlations. It is possible that these effects arise from the incomplete washout of CA^{4+} from cartilaginous tissues as previously described by Joshi et al.[33]

Aside from the present study, there is minimal data correlating quantitative imaging techniques to mechanical properties of the IVD. Ellingson et al[34] correlated T2* MRI to pure moment bending mechanics in cadaveric IVDs and found significant correlations of T2* imaging parameters to stiffness, range-of-motion, and neutral zone length. Their study further determined that multiple T2* parameters, which indirectly measure GAG content via free water content, were more predictive of IVD mechanics than Pfirrmann damage grade, corroborating the direct correlation of GAG content to IVD mechanical properties observed in the present study. In articular cartilage, Lakin et al[19–21] have established correlations between CE-μCT attenuation and mechanical properties of cartilage. In their study, bovine osteochondral plugs underwent CE-μCT imaging followed by unconfined compressive stress-relaxation and torsional tests, and CE-μCT attenuation was found to correlate highly to both equilibrium compressive modulus and coefficient of friction.[20] Follow-up studies in articular cartilage of the human metacarpal joint and murine tibial plateau produced similar findings.[19,21] Though the loading pattern differs considerably between articular cartilage and the IVD, the compressive mechanical properties of both tissues are highly dependent on GAG-mediated water retention, and in that context, this data agrees with the findings of the present study.

CE-μCT of the IVD has been previously demonstrated using both Hexabrix and CA^{4+}.[18] The contrast agent concentrations used in this study were independently optimized to maximize tissue contrast and thus are not equal between contrast agents. At the concentrations used in this study, CA^{4+} attenuation was more sensitive to changes in the GAG content of the NP, while Hexabrix was more sensitive to changes in the GAG content of the whole IVD, based on the slopes of the linear regressions. This is consistent with the mechanism of contrast enhancement of each agent—the greater affinity of CA^{4+} to the GAG-rich NP affords greater uptake and a much higher dynamic range of measurement in the NP compared to the AF, whereas the partial exclusion of Hexabrix from both the NP and AF produces a more comparable dynamic range in both tissues. Due to its higher net charge, and thereby higher interaction with negatively charged GAG, CA^{4+} is known to provide greater contrast at a given concentration compared with Hexabrix.[33,35]

This study was conducted in a rat model of the IVD, and our results should be interpreted in the context of this model. As the mechanical role of GAG in the IVD is relatively well-conserved across species, the findings

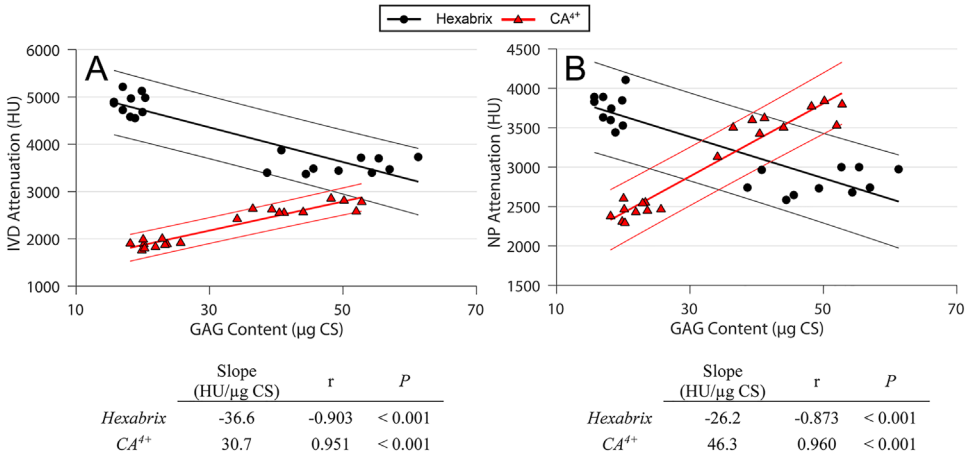

	Slope (HU/μg CS)	r	P
Hexabrix	-36.6	-0.903	< 0.001
CA4+	30.7	0.951	< 0.001

	Slope (HU/μg CS)	r	P
Hexabrix	-26.2	-0.873	< 0.001
CA4+	46.3	0.960	< 0.001

Figure 2. Correlation of GAG content, as determined by a DMMB assay, to IVD attenuation (A) and NP attenuation (B), shown with 95% confidence intervals. Correlation coefficients and *p*-values were determined using the Pearson product-moment correlation.

of this study should generally be applicable in larger species as well. However, translation of CE-μCT imaging into large animal and cadaveric human models would enable the indirect assessment of IVD mechanics described in this study to be applied in more clinically relevant scenarios. To date, CE-μCT has generally been applied as a research tool for rodent disease models, and while applications to articular cartilage in cadaveric and bovine models have been described,[19,20] applications to the IVD have thus far been limited to rabbits[14] and rats.[18,36] Translation into larger models is primarily limited by the increase in diffusion distance and subsequent increase in incubation time required to achieve equilibrium. This could potentially be circumvented via the use of mechanical convection,[37] incubation at higher temperature, or by other means.

This study should be interpreted in light of several limitations. An ex vivo enzymatic digestion model of DDD was used to induce GAG depletion. Though GAG depletion is the hallmark biochemical change associated with DDD, this model does not account for active remodeling of IVD tissue, cellular activity, nor for the concomitant changes to the vertebral endplates and vertebral bodies which are known to occur during DDD progression.[2,38] Future studies should confirm the observed correlations in in vivo models of DDD to account for these variables. As we did not perform in vivo μCT, and motion segments were extensively dissected prior to testing and analysis, determination of in situ IVD height was not possible given the absence of native muscle, tendon, and body weight forces acting on the dissected motion segment. To convert load/displacement to stress/strain data, we used μCT data and mechanical preconditioning data to calculate IVD height. This height, therefore, represents the "gauge length" of the final mechanical cycle and not the in situ height of the IVD. We performed whole motion segment mechanical testing as opposed to isolated characterization of the intrin-

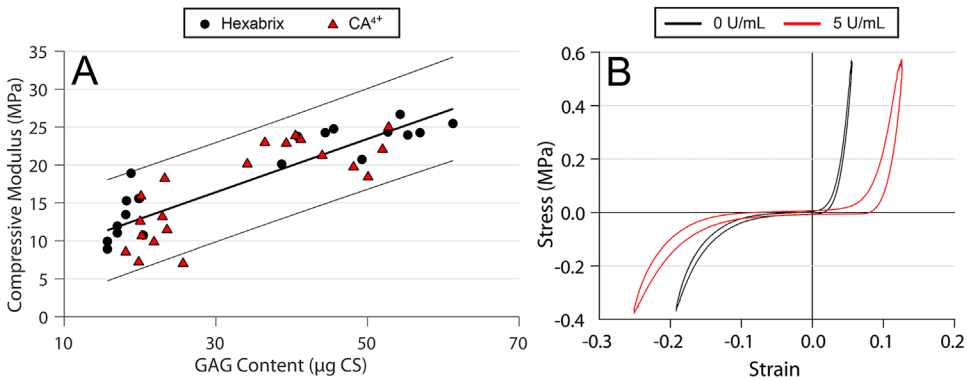

	Slope (MPa/μg CS)	r	P
Combined	0.35	0.855	< 0.001

Figure 3. Representative stress-strain of IVDs with (0 U/ml) or without (5 U/ml) enzymatic digestion in papain (A). Correlation of GAG content, as determined by DMMB assay, to compressive modulus (B), shown with 95% confidence intervals. Correlation coefficients and *p*-values were determined using the Pearson product-moment correlation.

Table 3. Correlation Statistics Between CE-μCT Attenuation and IVD Mechanical Properties

	Hexabrix Attenuation				CA^{4+} Attenuation			
	Whole IVD		NP		Whole IVD		NP	
Mechanical Parameter	*r*	*p*	*r*	*p*	*r*	*p*	*r*	*p*
Modulus								
Compressive	−0.884	<**0.001**	−0.909	<**0.001**	0.855	<**0.001**	0.876	<**0.001**
Tensile	−0.777	<**0.001**	−0.789	<**0.001**	0.483	**0.031**	0.485	**0.030**
Stiffness								
Compressive	−0.868	<**0.001**	−0.890	<**0.001**	0.882	<**0.001**	0.902	<**0.001**
Tensile	−0.667	<**0.001**	−0.698	<**0.001**	0.432	0.057	0.442	0.051
Hysteresis								
Compressive	0.876	<**0.001**	0.908	<**0.001**	−0.854	<**0.001**	−0.869	<**0.001**
Tensile	0.824	<**0.001**	0.863	<**0.001**	−0.177	0.455	−0.197	0.404
Total	0.868	<**0.001**	0.902	<**0.001**	−0.778	<**0.001**	−0.797	<**0.001**

Correlation coefficients and *p*-values were determined via the pearson product-moment correlation.

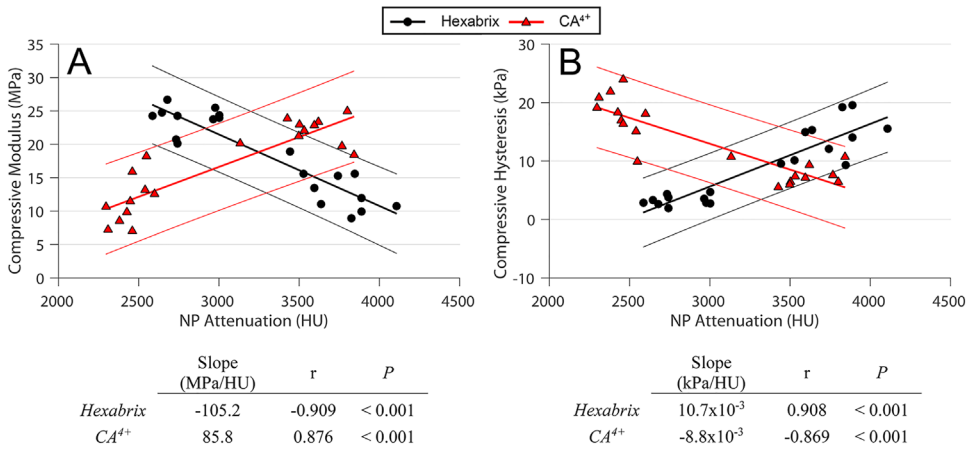

Figure 4. Correlation of NP attenuation to compressive modulus (A) and compressive hysteresis (B), shown with 95% confidence intervals. Correlation coefficients and *p*-values were determined via the Pearson product-moment correlation.

sic properties of IVD substructures/tissues. While this represents a more practical and translational approach for studies assessing pathology and regeneration, future studies may wish to specifically assess the inherent compressive properties of the NP to establish correlations to CE-μCT. Uniaxial cyclic testing was employed in this study. Though uniaxial loading is an important component of overall IVD loading, we did not assess other important motions, including bending and torsion. Asymmetric loading of the disc has been shown to induce decreased annular cellularity and subsequent repair in the disc region subjected to bending, and multiple studies have linked IVD bending to structural instability and perpetuation of IVD degeneration.[39,40] Future studies correlating CE-μCT to mechanical properties derived from these clinically relevant motion profiles are warranted.

Table 4. Mean Absolute Percentage Error (MAPE) Values From 100 Iterations of Repeated Random Sub-Sampling Cross Validation of Linear Regression Models Between CE-μCT Attenuation and IVD Mechanical Properties

	Hexabrix Attenuation		CA^{4+} Attenuation	
	Whole IVD	NP	Whole IVD	NP
Compressive Modulus	17.63% ± 3.23	14.85% ± 2.92	20.23% ± 5.59	19.87% ± 5.37
Compressive Stiffness	14.42% ± 2.70	14.05% ± 2.43	18.33% ± 3.51	16.79% ± 4.14

CONCLUSION

The purpose of this study was to determine whether CE-μCT attenuation of the IVD can be used as an indirect measure of IVD mechanical properties in an ex vivo model of DDD. The results of this study demonstrate that CE-μCT may represent an effective indirect and nondestructive modality for assessing the compressive properties of the IVD with high predictive accuracy.

AUTHORS' CONTRIBUTION

All authors have made substantial contributions to the conception and design of the study, acquisition of data, and/or analysis and interpretation of data, as well as manuscript preparation and final approval of the submitted manuscript. TM takes responsibility for the integrity of the work as a whole.

ACKNOWLEDGMENTS

The authors have no relevant conflicts of interest. Contrast agent synthesis was funded by the Department of Natural Sciences at Lawrence Technological University. All other experimentation was funded by the Department of Orthopaedic Surgery at Beaumont Health. The authors wish to thank the Lumigen Instrument Center at Wayne State University for the use of NMR and MS facilities, and Guerbet Inc. for the donation of Hexabrix 320.

REFERENCES

1. Zeckser J, Wolff M, Tucker J, et al. 2016. Multipotent mesenchymal stem cell treatment for discogenic low back pain and disc degeneration. Stem Cells International 2016:1–13.
2. Adams MA, Roughley PJ. 2006. What is intervertebral disc degeneration, and what causes it? Spine 31:2151–2161.
3. Urban JP, Roberts S. 2003. Degeneration of the intervertebral disc. Arthritis Res Ther 5:120.
4. Boxberger JI, Sen S, Yerramalli CS, et al. 2006. Nucleus pulposus glycosaminoglycan content is correlated with axial mechanics in rat lumbar motion segments. J Orthop Res 24:1906–1915.
5. Inoue N, Oŕas AAE. 2011. Biomechanics of intervertebral disk degeneration. Orthop Clin North Am 42:487–499.
6. Beckstein JC, Sen S, Schaer TP, et al. 2008. Comparison of animal discs used in disc research to human lumbar disc: axial compression mechanics and glycosaminoglycan content. Spine 33:E166–E173.
7. Raj PP. 2008. Intervertebral disc: anatomy-physiology-pathophysiology-treatment. Pain Pract 8:18–44.
8. Hukins D. 1992. A simple model for the function of proteoglycans and collagen in the response to compression of the intervertebral disc. Proc R Soc Lond B Biol Sci 249:281–285.
9. Johannessen W, Elliott DM. 2005. Effects of degeneration on the biphasic material properties of human nucleus pulposus in confined compression. Spine 30:E724–E729.
10. Michalek AJ, Funabashi KL, Iatridis JC. 2010. Needle puncture injury of the rat intervertebral disc affects torsional and compressive biomechanics differently. Eur Spine J 19:2110–2116.
11. Lotz JC. 2004. Animal models of intervertebral disc degeneration: lessons learned. Spine 29:2742–2750.
12. Elliott DM, Sarver JJ. 2004. Young investigator award winner: validation of the mouse and rat disc as mechanical models of the human lumbar disc. Spine 29:713–722.
13. Palmer AW, Guldberg RE, Levenston ME. 2006. Analysis of cartilage matrix fixed charge density and three-dimensional morphology via contrast-enhanced microcomputed tomography. Proc Natl Acad Sci USA 103: 19255–19260.
14. Maerz T, Newton M, Kristof K, et al. 2014. Three-dimensional characterization of in vivo intervertebral disc degeneration using EPIC-μCT. Osteoarthritis Cartilage 22: 1918–1925.
15. Xie L, Lin AS, Guldberg RE, et al. 2010. Nondestructive assessment of sGAG content and distribution in normal and degraded rat articular cartilage via EPIC-microCT. Osteoarthritis Cartilage 18:65–72.
16. Xie L, Lin AS, Kundu K, et al. 2012. Quantitative imaging of cartilage and bone morphology, reactive oxygen species, and vascularization in a rodent model of osteoarthritis. Arthritis Rheum 64:1899–1908.
17. Xie L, Lin AS, Levenston ME, et al. 2009. Quantitative assessment of articular cartilage morphology via EPIC-microCT. Osteoarthritis Cartilage 17:313–320.
18. Newton MD, Hartner SE, Timmons S, et al. 2016. Contrast-enhanced μCT of the intervertebral disc: a comparison of anionic and cationic contrast agents for biochemical and morphological characterization. J Orthop Res 49:4159–4163.
19. Lakin BA, Ellis DJ, Shelofsky JS, et al. 2015. Contrast-enhanced CT facilitates rapid, non-destructive assessment of cartilage and bone properties of the human metacarpal. Osteoarthritis Cartilage 23:2158–2166.
20. Lakin BA, Grasso DJ, Shah SS, et al. 2013. Cationic agent contrast-enhanced computed tomography imaging of cartilage correlates with the compressive modulus and coefficient of friction. Osteoarthritis Cartilage 21:60–68.
21. Lakin BA, Patel H, Holland C, et al. 2015. Contrast-enhanced CT using a cationic contrast agent enables non-destructive assessment of the biochemical and biomechanical properties of mouse tibial plateau cartilage. J Orthop Res 34:1130–1138.
22. Joshi NS, Bansal PN, Stewart RC, et al. 2009. Effect of contrast agent charge on visualization of articular cartilage using computed tomography: exploiting electrostatic interactions for improved sensitivity. JACS 131:13234–13235.
23. Chan SC, Burki A, Bonel HM, et al. 2013. Papain-induced in vitro disc degeneration model for the study of injectable nucleus pulposus therapy. Spine J 13:273–283.
24. Roberts S, Menage J, Sivan S, et al. 2008. Bovine explant model of degeneration of the intervertebral disc. BMC Musculoskelet Disord 9:24.
25. Boxberger JI, Auerbach JD, Sen S, et al. 2008. An in vivo model of reduced nucleus pulposus glycosaminoglycan content in the rat lumbar intervertebral disc. Spine 33:146.
26. Cannella M, Arthur A, Allen S, et al. 2008. The role of the nucleus pulposus in neutral zone human lumbar intervertebral disc mechanics. J Biomech 41:2104–2111.
27. Hutton W, Gharpuray V. 1998. The effect of fluid loss on the viscoelastic behavior of the lumbar intervertebral disc in compression. J Biomed Eng 120:48–54.
28. Panagiotacopulos ND, Pope MH, Bloch R, et al. 1987. Water content in human intervertebral discs: part II. viscoelastic behavior. Spine 12:918–924.
29. Han WM, Nerurkar NL, Smith LJ, et al. 2012. Multi-scale structural and tensile mechanical response of annulus fibrosus to osmotic loading. Ann Biomed Eng 40: 1610–1621.
30. Ebara S, Iatridis JC, Setton LA, et al. 1996. Tensile properties of nondegenerate human lumbar anulus fibrosus. Spine 21:452–461.

31. Skaggs D, Weidenbaum M, Ratcliffe A, et al. 1994. Regional variation in tensile properties and biochemical composition of the human lumbar anulus fibrosus. Spine 19:1310–1319.
32. Guerin HAL, Elliott DM. 2006. Degeneration affects the fiber reorientation of human annulus fibrosus under tensile load. J Biomech 39:1410–1418.
33. Bansal PN, Stewart RC, Entezari V, et al. 2011. Contrast agent electrostatic attraction rather than repulsion to glycosaminoglycans affords a greater contrast uptake ratio and improved quantitative CT imaging in cartilage. Osteoarthritis Cartilage 19:970–976.
34. Ellingson AM, Mehta H, Polly DW, Jr et al. 2013. Disc degeneration assessed by quantitative T2*(T2 star) correlated with functional lumbar mechanics. Spine 38:E1533–-E1540.
35. Bansal PN, Joshi NS, Entezari V, et al. 2011. Cationic contrast agents improve quantification of glycosaminoglycan (GAG) content by contrast enhanced CT imaging of cartilage. J Orthop Res 29:704–709.
36. Lin KH, Tang SY. 2017. The quantitative structural and compositional analyses of degenerating intervertebral discs using magnetic resonance imaging and contrast-enhanced micro-Computed tomography. Ann Biomed Eng 45:2626–2634.
37. Entezari V, Bansal PN, Stewart RC, et al. 2014. Effect of mechanical convection on the partitioning of an anionic iodinated contrast agent in intact patellar cartilage. J Orthop Res 32:1333–1340.
38. Benneker LM, Heini PF, Alini M, et al. 2005. 2004 Young Investigator Award Winner: vertebral endplate marrow contact channel occlusions and intervertebral disc degeneration. Spine 30:167–173.
39. Chin JR, Liebenberg E, Colliou OK, et al. 2007. Biological and mechanical consequences of transient intervertebral disc bending. Eur Spine J 16:1899–1906.
40. Court C, Colliou OK, Chin JR, et al. 2001. The effect of static in vivo bending on the murine intervertebral disc. Spine J 1:239–245.

SUPPORTING INFORMATION

Additional supporting information may be found in the online version of this article.